Int J Mater Form (2015) 8:45–57
DOI 10.1007/s12289-013-1146-7

ORIGINAL RESEARCH

Derivation of a forming limit stress diagram from an experimental FLC, and comparison of the two criteria when applied to FE simulation of a pressing using different yield functions

Alan R. Carr · Andy Walker · Etienne Combaz

Received: 17 April 2013 / Accepted: 3 September 2013 / Published online: 2 October 2013

Abstract The concept of a Forming Limit Curve (FLC), introduced in the sixties, has been widely used in the sheet metal industry, both to check out die designs at the design stage, using FE simulation techniques, and also to sign off stamped parts in the press shop. However, this approach should be strictly limited to stamping processes where the strain path is proportional during the stamping process. An alternative concept, the Forming Limit Stress Diagram (FLSD), was proposed back in the eighties. This FLSD concept is path independent, and solves the problem of possible non-linearity of the strain path during a press forming operation. The following paper uses a procedure for the transformation of an experimental path dependent strain based FLC into a stress based path independent FLSD, for three different yield functions, von Mises, Hill'48 and Hill's 90. Having derived the FLSD criterion, this paper then shows a comparison between the FE stamping simulations carried out on a selected component, using both the standard FLC approach and the more recent FLSD approach, using each one of the three different yield criterion considered. The FE simulation results using the FLSD transformation and the original FLC approach show good agreement for each of the yield functions considered. Some differences between the yield functions are also highlighted and discussed, in particular the limitations of Hill's 48 in the balanced bi-axial stress state for materials with an r value less than one, i.e. aluminium alloys.

A. R. Carr
Island of Rhodes, Greece

A. Walker
Novelis Switzerland SA, Route des Laminoirs 15, 3960 Sierre, Switzerland

E. Combaz (✉)
Novelis Innovation Center Sierre, Route des Laminoirs 15, 3960 Sierre, Switzerland
e-mail: etienne.combaz@novelis.com

Keywords Forming limit diagram · Forming limit stress diagram · Sheet metal forming · Yield function · Finite element stamping simulations

Introduction

Following the introduction of the concept of a Forming Limit Diagram (FLD), or a Forming Limit Curve (FLC), by Keeler& Backhofen [1] and Goodwin [2], this approach has been widely used in the sheet metal industry, both to check out die designs at the concept stage, using FE simulation techniques, and to sign off stamped parts in the press shop. Provided the strain paths of the stamped part are sensibly proportional during the stamping process, this technique can be used to good effect. However, it is known that the final position of the FLC depends upon the strain path undertaken to get to the end state point [3–6]. Hence, for a stamped part undergoing a variable strain path, the concept of an FLC becomes increasingly invalid the greater the degree of non-linearity of the strain path.

The concept of a Forming Limit Stress Diagram (FLSD), introduced by Arrieux et al. [7], and developed over time by a number of authors [8–15], has not been adopted throughout the sheet metal industry as was the case with the FLC approach. This is surprising in view of the fact that the FLSD is path independent, and eliminates the problem of possible non-linearity of the strain path during the press forming operation. However, experience has been very limited in applying the FLSD in the industry, and more experience needs to be built up over time by the stamping industry, perhaps running both criterion in parallel, to gain the necessary confidence in the FLSD approach.

In the following lines we briefly detailed the equations needed to apply the FLSD concept using the models actually still in used in industry. FE simulation of a pressing is then made comparing the various classical yield models used with the FLD and the FLSD criterion.

Basic theory and transformation of experimental FLC to stress space of the FLSD

Although the FLC failure criterion is normally displayed in strain space in the plane of (ε_1, ε_2), (true plastic strain neglecting the elastic portion), the failure criterion can be transformed to alternative planes using known formulae for plane stress plasticity [16]. Following a similar approach adopted by Bai & Wierzbicki [17], strain and stress ratio are defined respectively as:

$$\beta = d\varepsilon_2/d\varepsilon_1$$

and

$$\alpha = \sigma_2/\sigma_1$$

with

$$\sigma_3 = 0$$

for plane stress present in thin sheet deformation. In introducing the symbols for the stress and strain ratios, the authors are conscience of the fact that various authors have adopted the same notation used here, whereas numerous other authors have adopted the opposite usage of α and β.

Now it follows that:

$$\sigma_2 = \alpha\sigma_1 \tag{1}$$

Also,

$$d\varepsilon_2 = \beta d\varepsilon_1 \tag{2}$$

Also from volume constancy it can be shown that:

$$d\varepsilon_3 = -(1+\beta)d\varepsilon_1 \tag{3}$$

von Mises yield function

A relationship between the stress ratio α and the strain ratio β can be obtained by substituting the above equations for the strain increments, together with that for σ_2, into the Levy-Mises equations below [18]

$$d\varepsilon_1 = \left(d\bar{\varepsilon}/\bar{\sigma}\right)[\sigma_1 - 0.5(\sigma_2+\sigma_3)] \text{and } d\varepsilon_2 = \left(d\bar{\varepsilon}/\bar{\sigma}\right)[\sigma_2 - 0.5(\sigma_1+\sigma_3)]$$

giving the following well known equations:

$$\alpha = (1+2\beta)/(2+\beta) \tag{4}$$

$$\beta = (1-2\alpha)/(\alpha-2) \tag{5}$$

The increment of equivalent strain is defined in terms of the incremental plastic strain components:

$$d\bar{\varepsilon} = \left(2^{1/2}/3\right)\left[(d\varepsilon_1 - d\varepsilon_2)^2 + (d\varepsilon_2 - d\varepsilon_3)^2 + (d\varepsilon_3 - d\varepsilon_1)^2\right]^{1/2} \tag{6}$$

Substitution of Eqs. (2) and (3) into Eq. (6) gives the increment of equivalent strain in terms of the strain ratio β:

$$d\bar{\varepsilon} = \left(2/3^{1/2}\right)d\varepsilon_1\left[1+\beta+\beta^2\right]^{1/2} \tag{7}$$

Under the proportional loading of plane stress conditions, the strain ratio is constant, and Eq. (7) may be integrated to give:

$$\bar{\varepsilon} = \left(2/3^{1/2}\right)\varepsilon_1\left[1+\beta+\beta^2\right]^{1/2} \tag{8}$$

Now introducing the von Mises Yield function [19]:

$$\bar{\sigma} = \left(1/2^{1/2}\right)\left[(\sigma_1 - \sigma_2)^2 + (\sigma_2 - \sigma_3)^2 + (\sigma_3 - \sigma_1)^2\right]^{1/2} \tag{9}$$

and substituting the stress ratio α, Eq. (1), together with σ_3 = zero for plane stress, gives:

$$\bar{\sigma} = \sigma_1\left[1 - \alpha + \alpha^2\right]^{1/2} \tag{10}$$

Hence:

$$\sigma_1 = \bar{\sigma}/\left[1 - \alpha + \alpha^2\right]^{1/2} \tag{11}$$

$$\sigma_2 = \alpha\bar{\sigma}/\left[1 - \alpha + \alpha^2\right]^{1/2} \tag{12}$$

It is now necessary to introduce a constitutive law to define the material's work-hardening behaviour. Bai &Wierzbicki [17] introduced a simple power law, (which is more applicable to various steels), to describe the materials work-hardening behaviour.

$$\bar{\sigma} = A\bar{\varepsilon}^n \tag{13}$$

In the current paper, which relates to an aluminium material, all presented and discussed results have been based upon

a saturation stress Voce equation model, fitted to the measured tensile test data. This one may not be the best model but it is widely used in industry as it present the safest model and produce accurate enough fit to experimental tensile flow curve.

$$\overline{\sigma} = A + Be^{C\bar{\varepsilon}} \tag{14}$$

The Voce equation Eq. (14) can now be directly substituted into Eqs. (11) and (12) giving:

$$\sigma_1 = \left(A + Be^{C\bar{\varepsilon}}\right) / \left[1 - \alpha + \alpha^2\right]^{1/2} \tag{15}$$

$$\sigma_2 = \alpha\left(A + Be^{C\bar{\varepsilon}}\right) \sigma / \left[1 - \alpha + \alpha^2\right]^{1/2} \tag{16}$$

Starting from the experimental plastic strain pairs defining the FLC, $\varepsilon_1 : \varepsilon_2$, it is possible to transpose the FLC into the FLSD. For a given strain data pair, the strain ratio is known from the experimental strain points, and hence the stress ratio can be determined from Eq. (4). The principal stresses can then be solved using Eqs. (15) and (16), together with Eq. (8).

When the procedure of Bai &Wierzbicki [17] was followed, but using the saturation Voce equation Eq. (14) instead of a simple power law, a "convex" shaped FLSD was obtained – see Figs. 1 and 2 below. This differs from the normal "concave" shaped FLSD in literature, [3] and [17].

In this paper, all FE simulations were conducted using the code PamStamp, version 2G v2012.0.

FE analysis was carried out on a simple pressing to assess the correlation between the conventional strain based FLC criterion and the stress based FLSD criterion. The results are shown in Figs. 3 and 4.

As mentioned previously, the FE simulation work was conducted using a Voce equation saturation stress constituency model of the form:

$$\overline{\sigma} = A + Be^{\overline{C\bar{\varepsilon}}} \tag{17}$$

where "e" is the natural logarithm base. For the Ac170PX material under consideration, (alloy AA6014), the constants of the Voce equation, when fitted to the measured tensile test data, were evaluated as:

$$A = 297.3780 \quad B = -178.4069 \quad C = -11.68287$$

In the current analysis, experimentally determined plastic strain pairs defining the FLC, $\varepsilon_1 : \varepsilon_2$, were transposed onto the FLSD. A safety margin offset of −0.08 was applied to the major strain ε_1 and introduced into the FLC diagram to define

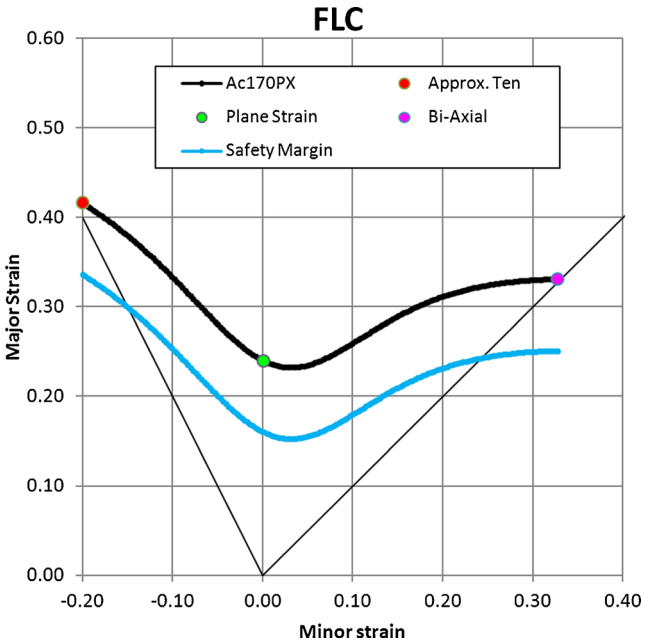

Fig. 1 Experimental FLC

the marginal zone. It is normal practice to define an offset for the marginal zone, although the magnitude of the offset may vary. This safety margin has also been transposed into the FLSD using the same procedure as outlined for the FLC.

The results of the FE simulation work, shown in Figs. 3 and 4, show very good agreement between the conventional FLC analysis and the transposed FLSD analysis. The marginal and failed areas in the central dome and the right hand upper corner, (i.e. at the plane strain tangent point of the punch

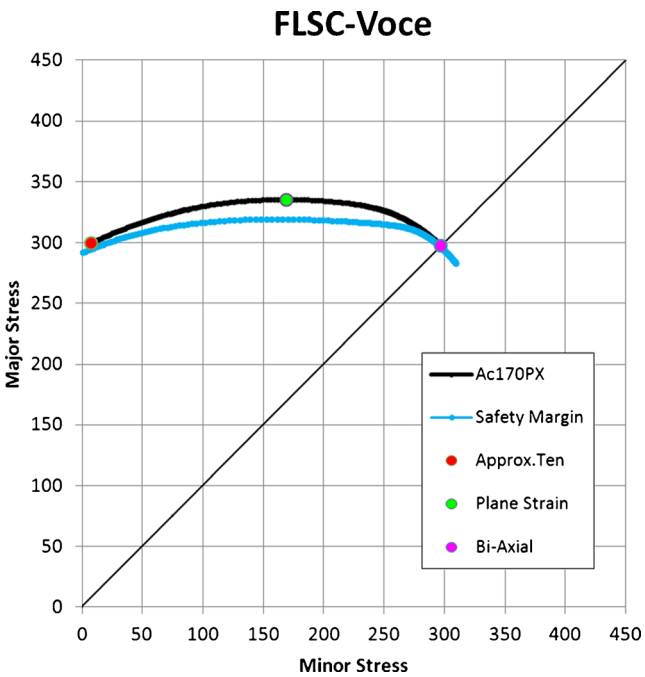

Fig. 2 Transposed FLC into FLSD — von Mises

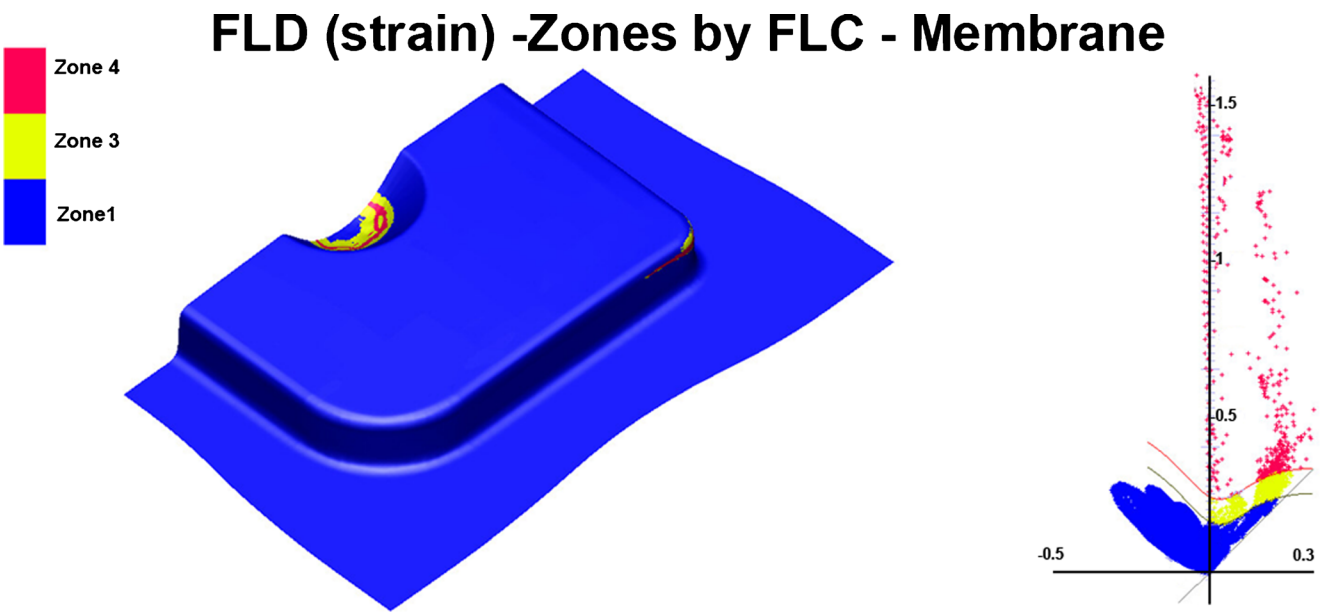

Fig. 3 FE simulation conducted using von Mises yield criterion with FLC Criterion

radius), are reproduced very well in both Figs. 3 and 4. However, the FLSD criterion shows additional marginal zones around the die entry radius of the two corner features. These marginal zones are not present in the FLC analysis. This is particularly interesting as one can occasionally observe, in practice, stress related fractures in the area of the die entry corner radius where the conventional FLC strain analysis does not show any associated problems.

The reason that the FLC approach does not pick up this marginal area may be related to the strain path change as the material moves over the hold down/binder area towards the die corner under plane strain conditions $\varepsilon_1 : \varepsilon_2$, (constant thickness in the binder clamping region), towards plane strain tension conditions in the side wall $\varepsilon_1 : \varepsilon_3$ during additional forming.

One additional point which should be noted is that the offset in the strain based FLC, in this case −0.08, maps to a much smaller region in the FLSD. Some concerns regarding the use of a stress criterion within the FE calculation were that the resolution in stress is less accurate in the code than the resolution in strain. Although the mapped marginal zone is somewhat smaller in the FLSD, the FE code and the analysis carried out to date have not highlighted any issues in resolving the element stresses to the necessary level of accuracy, and

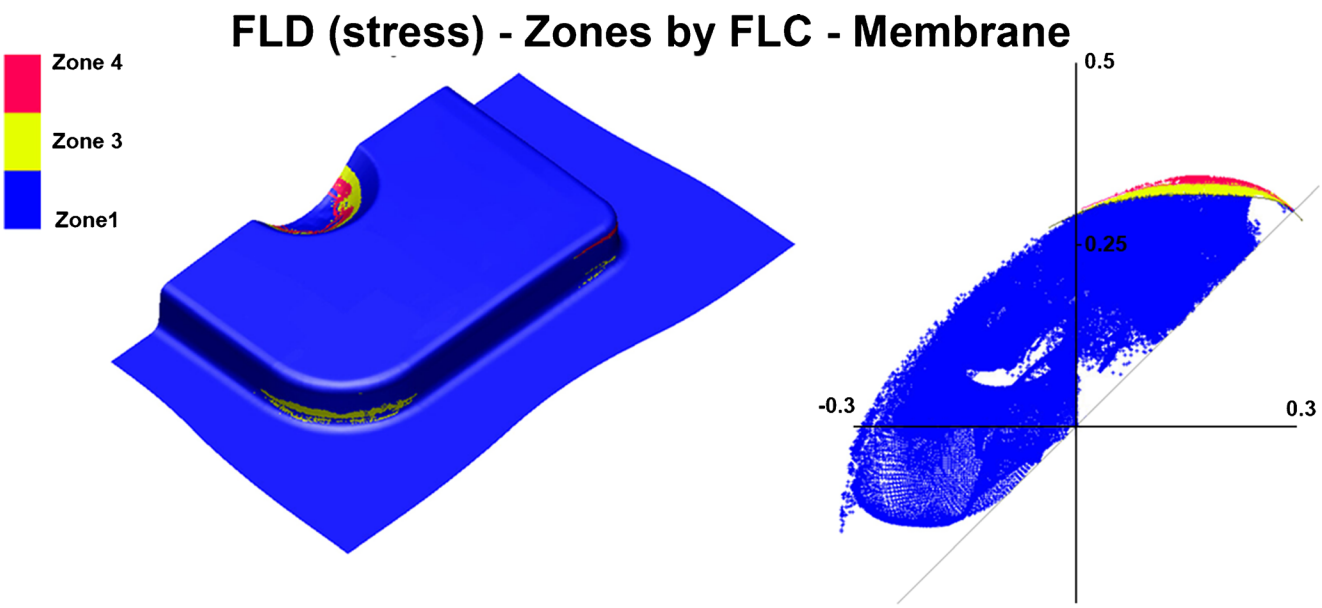

Fig. 4 FE simulation conducted using von Mises yield criterion with FLSD Criterion

hence in predicting the safe, marginal and failed areas on the pressing.

Hill's 48 yield function

Following on from the work discussed above for the von Mises yield function, Hill'48yield function will now be considered.

Hill's 48 yield function can be stated in the following form [20, 21]:

$$\overline{\sigma} = \frac{[3]^{1/2}}{[2]^{1/2}} \frac{\left[H(\sigma_1-\sigma_2)^2 + F(\sigma_2-\sigma_3)^2 + G(\sigma_3-\sigma_1)^2\right]^{1/2}}{[F+G+H]^{1/2}} \tag{18}$$

where r = (H/G) = (H/F), i.e. a sheet with rotational symmetry about the through thickness axis.

This can be restated assuming rotational symmetry in the plane of the sheet, (planar isotropic), and also for plane stress conditions, as:

$$\overline{\sigma} = \frac{[3]^{1/2}}{[2]^{1/2}} \frac{\left[r(\sigma_1-\sigma_2)^2 + {\sigma_2}^2 + {\sigma_1}^2\right]^{1/2}}{[2+r]^{1/2}} \tag{19}$$

Equation (1) may be substituted into Eq. (19) to define the yield function in terms of the stress ratio α as:

$$\overline{\sigma} = \frac{[3]^{1/2}}{[2]^{1/2}} \frac{\sigma_1}{[2+r]^{1/2}}\left[\alpha^2(1+r)-2\alpha r + (1+r)\right]^{1/2} \tag{20}$$

Rearranging Eq. (20) and substituting the saturation stress Voce equation, Eq. (17), gives the expression for the maximum principal stress as:

$$\sigma_1 = \frac{(A+Be^{C\bar{\varepsilon}})[2]^{1/2}[2+r]^{1/2}}{[3]^{1/2}[\alpha^2(1+r)-2\alpha r + (1+r)]^{1/2}} \tag{21}$$

The corresponding expression for the minor principal stress can be obtained by substituting Eq. (1) into Eq. (21), giving:

$$\sigma_2 = \frac{\alpha(A+Be^{C\bar{\varepsilon}})[2]^{1/2}[2+r]^{1/2}}{[3]^{1/2}[\alpha^2(1+r)-2\alpha r + (1+r)]^{1/2}} \tag{22}$$

The corresponding expression for the equivalent plastic strain, from Johnson & Mellor [21], can be stated as:

$$\varepsilon = \frac{[2]^{1/2}}{[3]^{1/2}} \frac{(2+r)^{1/2}}{(1+2r)}\left[(\varepsilon_2-r\varepsilon_3)^2 + (\varepsilon_1-r\varepsilon_3)^2 + r(\varepsilon_1-\varepsilon_2)^2\right]^{1/2} \tag{23}$$

Now following the same procedure outlined in "von Mises yield function" section, Hill's 48 yield function, Eq. (20), can be substituted in place of the von Mises yield function Eq. (10), and Hill's 48 equivalent plastic strain, Eq. (23), in place of Eq. (8). It will of course be necessary to redefine the stress and strain ratios, α and β, to be used in conjunction with Hill's 48 yield function. These expressions have been taken from the work of Stoughton [16], as:

$$\alpha = [(1+r)\beta + r]/(1+r+r\beta) \tag{24}$$

$$\beta = [(1+r)\alpha - r]/(1+r-r\alpha) \tag{25}$$

Note: for the aluminium material being evaluated in this paper, the r value distribution was measured as follows:

$$r_0 = 0.78 \quad r_{45} = 0.49 \quad r_{90} = 0.68$$

and $r_{average} = 0.61$ from the well know expression $r_{av} = (r_0 + r_{90} + 2r_{45})/4$

Starting from the known experimentally determined plastic strain pairs defining the FLC, $\varepsilon_1 : \varepsilon_2$, the FLC was transposed into the FLSD. For a given strain data pair, the strain ratio is known from the experimental measured instability strain points, and hence the stress ratio can be determined from Eq. (24). The stresses may then be solved using Eqs. (21) and (22), together with Eq. (23). The analysis, shown in Figs. 5 and 6, again shows a "convex" shaped FLSD. The safety margin of −0.08 has been included in the FLC diagram, and has also been transposed to the FLSD.

It again should be noted that the offset in the strain based FLC, in this case −0.08, maps to a much smaller region in the FLSD. However, the FE Code and the analysis carried out to date have not highlighted any issues in resolving the element stresses to the necessary level of accuracy, and hence in predicting the safe, marginal and failed areas on the pressing.

FE analysis was again carried out on a simple pressing, used in "von Mises yield function" section, to assess the correlation between the conventional strain based FLC criterion and the stress based FLSD criterion. The results are shown in Fig. 7 for the FLC criterion and Fig. 8 for the FLSD criterion.

The agreement can be seen to be good, particularly in the area of the right hand punch radius. However, it can be seen that there is no failure predicted in the central dome when using the FLSD criterion, Fig. 8. The reduced marginal zone areas and lack of any failure zones in the central dome under bi-

axial stress state conditions, when using the FLSD criterion, is perhaps understandable as it is known that Hill's 48 yield function gives a relatively poor representation of the stresses at the balanced bi-axial stress state for materials with r values less than one, i.e. aluminium alloys. The poor description of the yield function will in fact result in lower stresses than are present in practice. In fact this is one reason why Hill developed his subsequent non-quadratic yield function. This point will be discussed further in "Hill's 90 yield function" section of this paper when considering Hill's 90 criterion.

Additionally, the FLSD criterion is again showing marginal zones around the die entry radius of the lower left hand corner, highlighting possible stress fractures around the die inlet radius. This is not highlighted in the FLC analysis probably due to the strain path change, as discussed in "Hill's 48 yield function" section.

Hill's 90 yield function

Following on from the work discussed above, for both the von Mises and Hill's 48 yield functions, Hill's 90 yield function will now be considered.

Hill's 90 yield function [22] and [16] may be stated in the form:

$$\overline{\sigma} = \frac{1}{[2(1+\mathrm{r})]^{1/\mathrm{m}}}\left[(1+2\mathrm{r})|\sigma_1-\sigma_2|^{\mathrm{m}} + |\sigma_1+\sigma_2|^{\mathrm{m}}\right]^{1/\mathrm{m}} \quad (26)$$

where r is the average plastic anisotropy in the plane of the sheet. Equation (1) may be substituted into Eq. (26) to define the yield function in terms of the stress ratio α giving:

$$\overline{\sigma} = \frac{\sigma_1}{[2(1+\mathrm{r})]^{1/\mathrm{m}}}\left[(1+2\mathrm{r})|1-\alpha|^{\mathrm{m}} + |1+\alpha|^{\mathrm{m}}\right]^{1/\mathrm{m}} \quad (27)$$

Rearranging Eq. (27) and substituting the saturation stress Voce equation, Eq. (17), gives the expression for the maximum principal stress as:

$$\sigma_1 = \frac{(\mathrm{A}+\mathrm{Be}^{\mathrm{C}\bar{\varepsilon}})[2(1+\mathrm{r})]^{1/\mathrm{m}}}{\left[(1+2\mathrm{r})|1-\alpha|^{\mathrm{m}} + |1+\alpha|^{\mathrm{m}}\right]^{1/\mathrm{m}}} \quad (28)$$

The minor principal stress can be obtained by substituting Eq. (1) into Eq. (28), giving:

$$\sigma_2 = \frac{\alpha(\mathrm{A}+\mathrm{Be}^{\mathrm{C}\bar{\varepsilon}})[2(1+\mathrm{r})]^{1/\mathrm{m}}}{\left[(1+2r)|1-\alpha|^{\mathrm{m}} + |1+\alpha|^{\mathrm{m}}\right]^{1/m}} \quad (29)$$

The corresponding expression for the equivalent plastic strain [16] is given by:

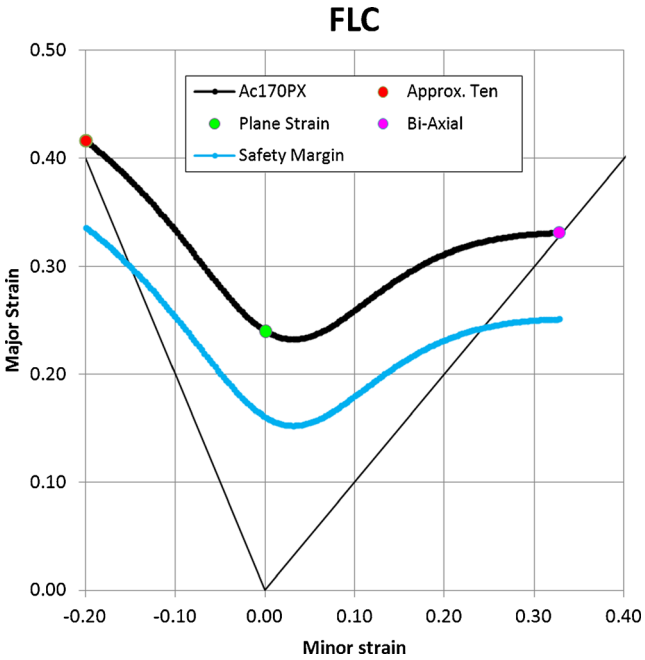

Fig. 5 Experimental FLC

$$\varepsilon = \frac{[2(1+\mathrm{r})]^{1/\mathrm{m}}}{2}\left[\left\{\left(|\varepsilon_1-\varepsilon_2|^{\mathrm{m}/(\mathrm{m}-1)}\right)/(1+2\mathrm{r})^{1/(\mathrm{m}-1)}\right\} + |\varepsilon_1+\varepsilon_2|^{\mathrm{m}/(\mathrm{m}-1)}\right]^{(\mathrm{m}-1)/\mathrm{m}} \quad (30)$$

Now following the same procedure outlined in "von Mises yield function" section, Hill's 90 yield function, Eq. (27) can be substituted in place of the von Mises Yield Criteria Eq (10),

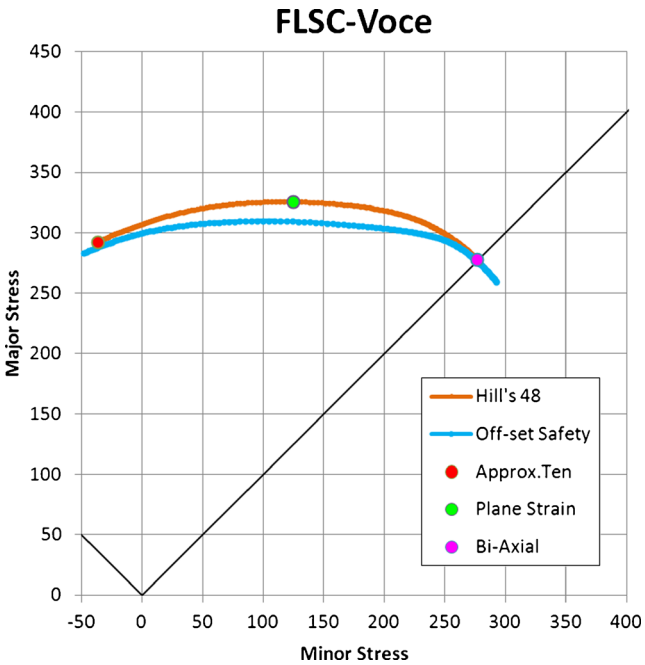

Fig. 6 Transposed FLC into FLSD

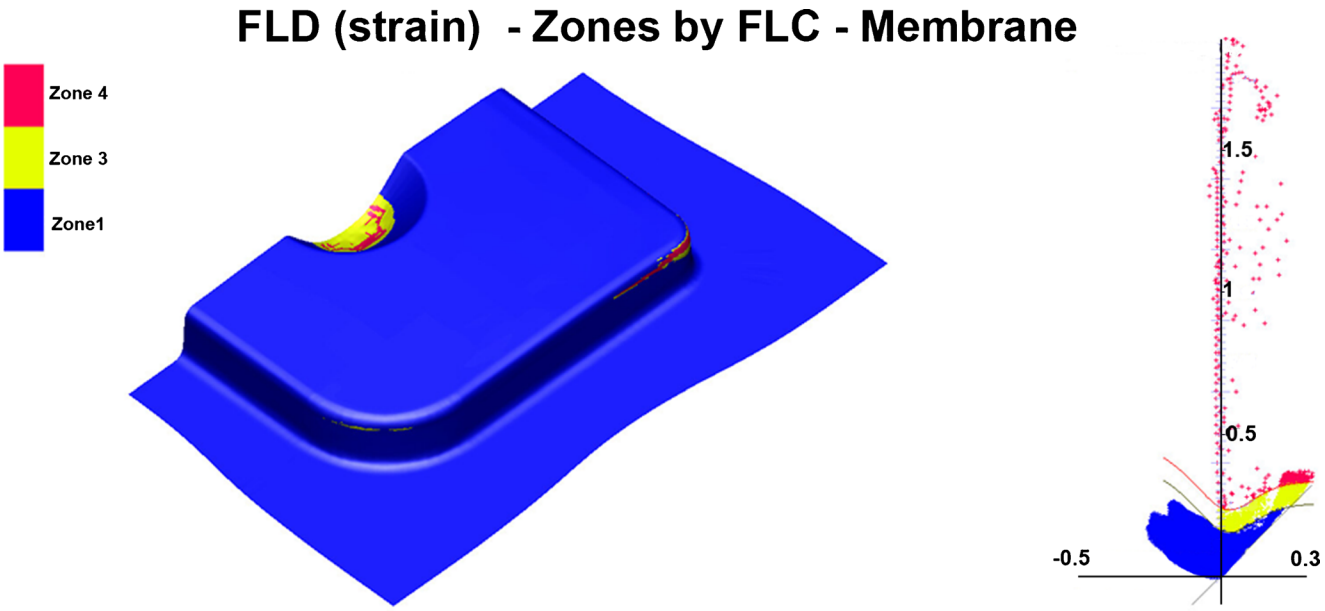

Fig. 7 FE simulation conducted using hill's 48 yield criterion with FLC criterion

and Hill's 90 equivalent plastic strain, Eq. (30), in place of Eq. (8). Once again it will be necessary to redefine the stress and strain ratios, α and β, to be used in conjunction with Hill's 48 yield function. These expressions have been taken from the work of Stoughton [16], as:

$$\alpha = \frac{[(1+2r)(1+\beta)]^{1/(m-1)} - (1-\beta)^{1/(m-1)}}{[(1+2r)(1+\beta)]^{1/(m-1)} + (1-\beta)^{1/(m-1)}} \tag{31}$$

$$\beta = \frac{(1+\alpha)^{(m-1)} - (1+2r)(1-\alpha)^{(m-1)}}{(1+\alpha)^{(m-1)} + (1+2r)(1-\alpha)^{(m-1)}} \tag{32}$$

Following the same procedure as outlined previously, and starting from known experimentally determined plastic strain pairs defining the FLC, $\varepsilon_1 : \varepsilon_2$, the FLC was transposed into the FLSD. For a given strain data pair, the strain ratio is known from the experimental measured instability strain points, and hence the stress ratio can be derived from Eq. (31). The stresses can then be obtained using Eqs. (28), (29) and (30). The analysis, shown in Figs. 9 and 10, again shows a "convex" shaped FLSD. A safety margin of −0.08 has been included in the FLC diagram, and has also been transposed to the FLSD.

As highlighted previously, it should be noted that the offset in the strain based FLC, in this case −0.08, maps to a much

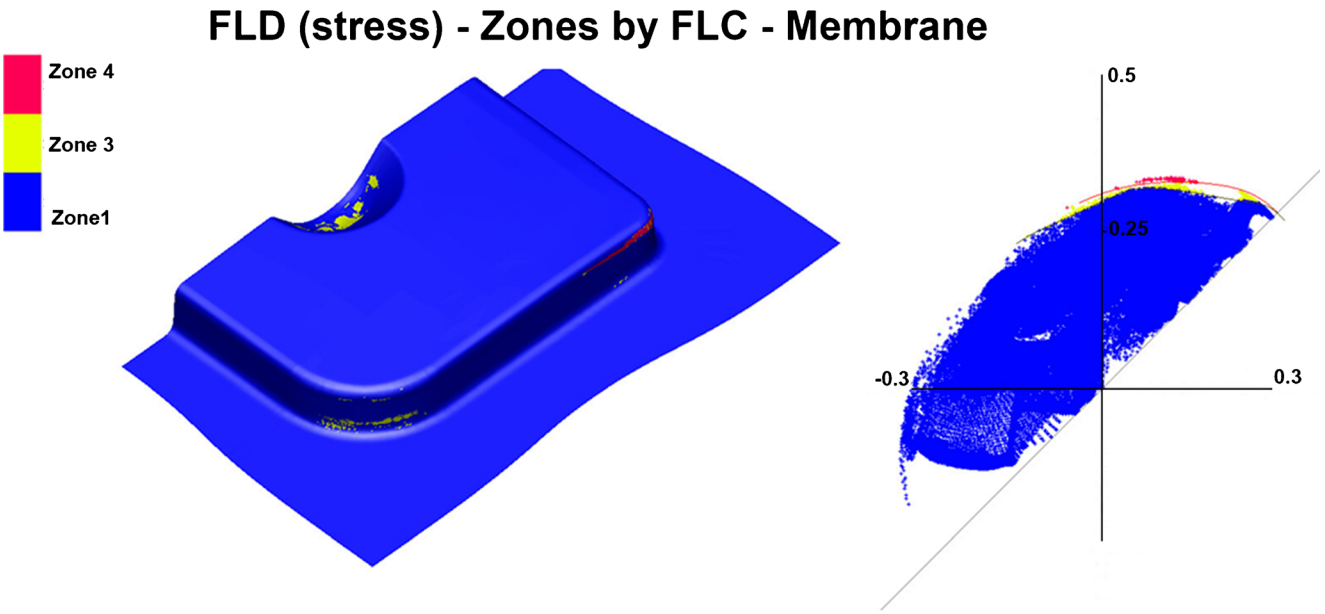

Fig. 8 FE simulation conducted using hill's 48 yield criterion with FLSD criterion

smaller region in the FLSD. However, the FE Code and the analysis carried out to date have not highlighted any issues in resolving the element stresses to the necessary level of accuracy, and hence in predicting the safe, marginal and failed areas on the pressing.

In order to determine the appropriate value of the power "m" in Hill's 90 yield function, it was necessary to compare the experimentally determined bi-axial stress–strain data with a prediction of the bi-axial data from the yield function. This was achieved by using the measured tensile stress–strain data to predict the bi-axial stress–strain data through Hill's 90 yield function, and selecting the best fit m value, as follows:

For the case of balanced bi-axial tension, $\sigma_1 = \sigma_2 = \sigma_B$. Substituting these values into Hill's 90 yield criterion, Eq. 26, gives:

$$\overline{\sigma} = \frac{2}{[2(1+r)]^{1/m}}\sigma_B \tag{33}$$

Also, for simple tension, $\sigma_1 = \sigma_T$ and σ_2 = zero. Substituting these values in Eq. 26 gives the expected result:

$$\overline{\sigma} = \sigma_T \tag{34}$$

From Eqs. 33 and 34 an expression can now be obtained to predict the balanced bi-axial stress data from the measured tensile data, via the yield function:

$$\sigma_B = \frac{[2(1+r)]^{1/m}}{2}\sigma_T \tag{35}$$

A similar approach can now be adopted to predict the bi-axial strain from the measured tensile strain by way of the yield function. For the case of balanced bi-axial tension, $\varepsilon_1 = \varepsilon_2$, and $\varepsilon_3 = \varepsilon_B = -2\varepsilon_1$. Substituting these values into Eq. 30 gives:

$$\overline{\varepsilon} = \frac{[2(1+r)]^{1/m}}{2}\varepsilon_3 = \frac{[2(1+r)]^{1/m}}{2}\varepsilon_B \tag{36}$$

Also, for simple tension:

$r = (\varepsilon_2/\varepsilon_3)$ and from volume constancy $\varepsilon_1 + \varepsilon_2 + \varepsilon_3 = 0$, hence

$$(\varepsilon_1/\varepsilon_3) = -(1+r) \quad \text{and} \quad (\varepsilon_1/\varepsilon_2) = \frac{-(1+r)}{r} \tag{37}$$

Substitution of Eq. 37 in Eq. 30 gives the expected result:

$$\overline{\varepsilon} = \varepsilon_1 = \varepsilon_T \tag{38}$$

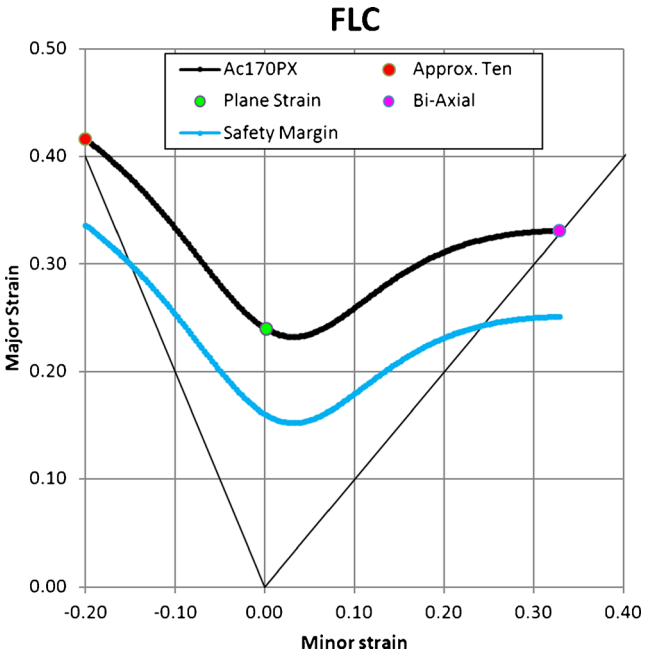

Fig. 9 Experimental FLC

Equations 36 and 38 now give the corresponding expression to predict the bi-axial strain, from the measured tensile strain data, via the yield function:

$$\varepsilon_B = \frac{2}{[2(1+r)]^{1/m}}\varepsilon_T \tag{39}$$

Using Eqs. 35 and 39, the prediction of the bi-axial stress–strain behaviour from the measured tensile data can now be

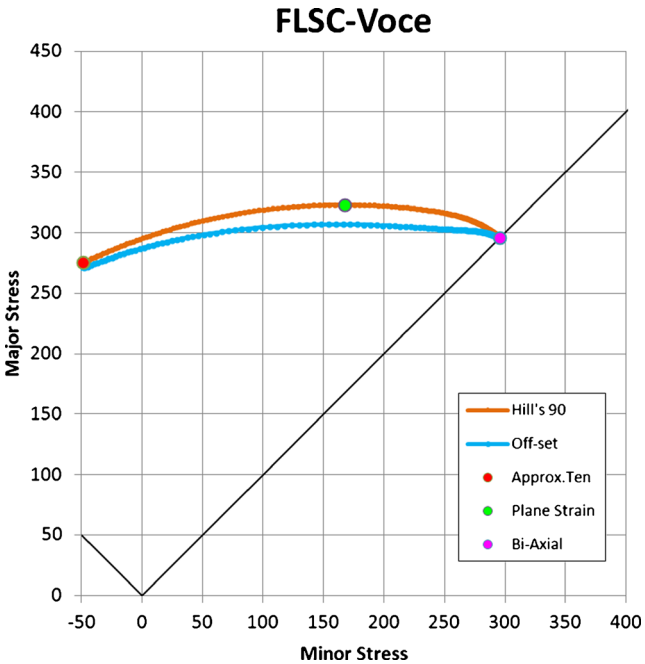

Fig. 10 Transposed FLC into FLSD

calculated and plotted along with the measured bi-axial stress–strain data. By varying the power m, the most appropriate value of the non quadratic yield function power can be selected — See Fig. 11.

As can be seen from Fig. 11, a value of m = 1.7 gives a very good fit between the measured bi-axial stress strain data, (red line) and the corresponding predicted data via the yield function using the measured tensile data, (black line). In fact for an m value of 1.7, the two lines are virtually coincident.

The measured tensile data, (light blue), although not visible, is directly below the predicted m = 1.7 line (black).

FE analysis was again conducted on the same pressing, used in Sections "von Mises yield function" and "Hill's 48 yield function", using both the FLC and the FLSD criteria. The results are shown in Fig. 12 for the FLC criterion and Fig. 13 for the FLSD criterion.

The agreement can again be seen to be very good, particularly in the area of the right hand punch radius and the central dome, where both FLC and FLSD criteria show very similar failed areas. The central dome FLSD red failure zones, when applying Hill's 90 yield function, contrasts the lack of failed zones when using Hill's 48 yield function in "Hill's 48 yield function" section. This difference may be understood from Fig. 11 by comparing the plots for m = 1.7, derived for Hill's 90, together with the m = 2 plot, which converts Hill's 90 into a quadratic yield function similar to the 48 yield function. The lower predicted stress levels at the bi-axial stress state using Hill's 48 would necessarily predict a non failed region as compared to the transposed FLC – FLSC criterion. This can be illustrated by comparing the yield surfaces for the different yield functions — Fig. 14.

The influence of decreasing the magnitude of the m value in Hill's 90 yield function is illustrated in Fig. 15. This shows that as the m value is decreased, the Yield Function is "stretched" to a greater degree in the bi-axial state, so obtaining a better prediction of the balanced bi-axial stress–strain behaviour, as is observed in practice.

Now referring back to Fig. 13, the FLSD criterion for Hill's 90 shows both marginal and failure zones around the die entry radius of the lower left hand corner. This is not evidenced in the FLC analysis, and is again an important indicator of possible stress fractures which can occasionally occur in die entry corner areas. As discussed previously in "von Mises yield function" section, the reason that the FLC approach does not highlight this marginal area may be related to the strain path change as the material moves over the hold down/binder area towards the die corner under plane strain conditions $\varepsilon_1 : \varepsilon_2$, (constant thickness in the binder clamping region), towards plane strain tension conditions in the side wall $\varepsilon_1 : \varepsilon_3$ during additional forming.

The FLC approach, when using all three yield functions, predicts no marginal or failed areas in the region of the die entry corner, Figs. 3, 7, and 13. However, FLSD approach when

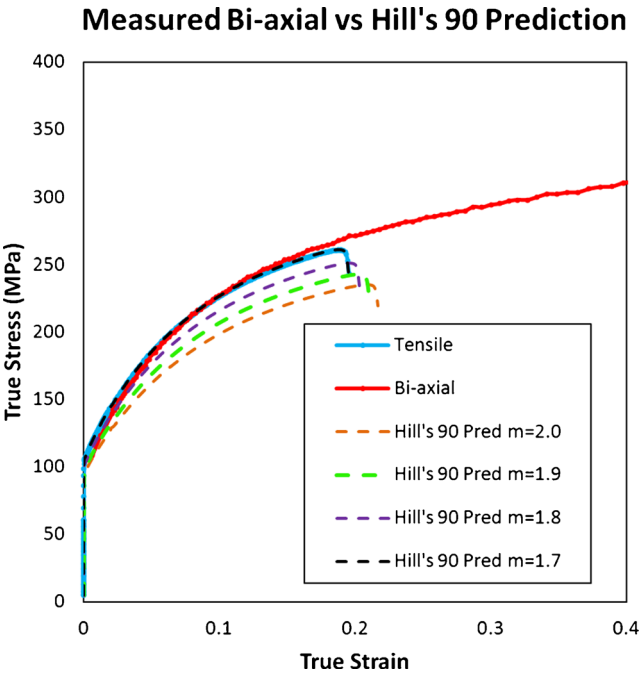

Fig. 11 Hill's 90 Yield Function with different m values showing good agreement with m = 1.7. *Note*: Tensile data lies directly under the value of m = 1.7

using the von Mises and Hill'48 functions predicts marginal areas in the region of the die entry corner, Figs. 4 and 8, whilst Hill's 90 predicts a failure in this region, Fig. 13. Firstly, the FLSD analysis in this area should be more accurate due to a strain path change over the die entry radius, which will not be captured accurately in the FLC analysis due to the strain path change. Hence a cautious approach would need to be applied to the design of the component in this area. Secondly, the different severity of the predictions shown in the region of the die entry corner area, when applying the three yield functions considered, should be investigated experimentally to resolve the accuracy of the predictions from the FE analysis, and hence the accuracy of the three different yield functions in describing correctly the yield surface of the material considered.

One final point should be noted as follows. When starting from a unique measured proportional strain path FLC, the resulting FLSD will necessarily depend upon the assumed yield function, as well as the assumed material constituency law. Figure 16 shows the difference in the transposed FLSD criteria, when starting from the same FLC data pairs, as a function of the three different yield functions considered in this paper. In all cases the material constituency law was the saturation Voce equation fitted to the measured tensile test data.

Right use of these FLSD implies to use only the same material model in the simulation as was used to derive the FLSD. If an FE analysis is conducted by selecting a given yield criterion, say Hill's 90, but an FLSD criterion derived from the

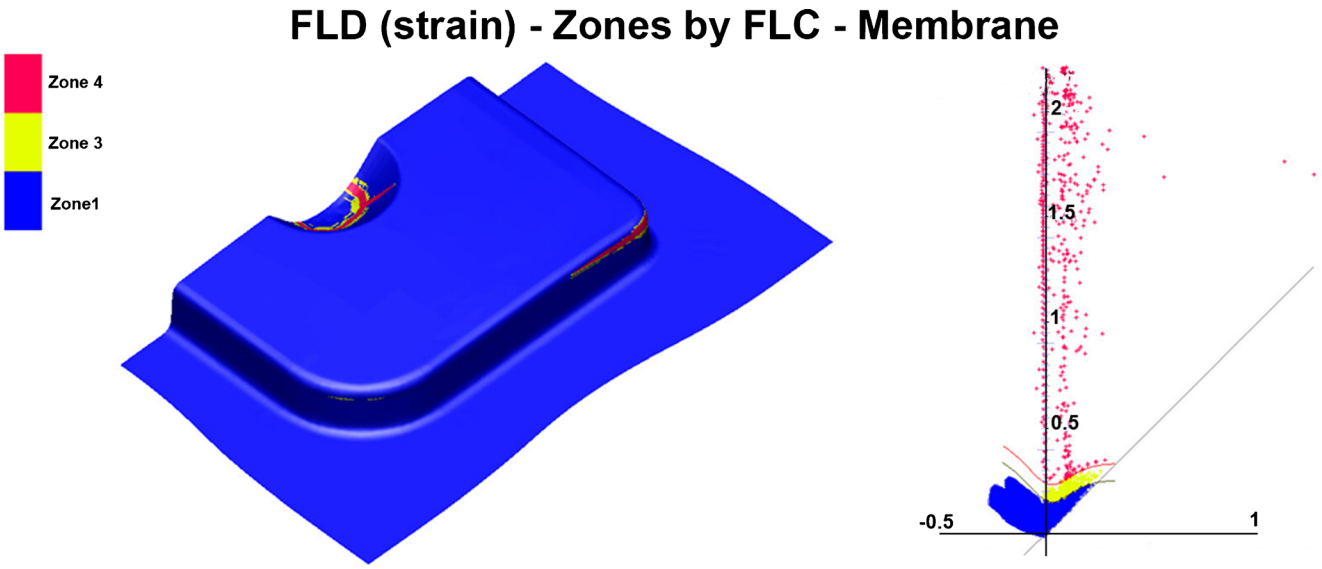

Fig. 12 FE simulation conducted using hill's 90 yield criterion with FLC criterion

von Mises is adopted as the safe/marginal/failure criterion, then erroneous results will be obtained which could be very misleading.

Standard FLC together with instability strains determined from a pre-strained material, with subsequent mapping to an FLSD using the von Mises yield function

As discussed in the Introduction, if a significant deviation from a linear or proportional strain path occurs, the final instability strains will be different to those obtained by a linear or proportional strain path FLC approach. Figure 17, (LHS), shows the influence of a 15 % tensile pre-strain on the final instability strains [13], (in red), as compared to the conventional FLC, (in black). Figure 17 (RHS) shows the transposed data to the FLSD using the von Mises yield function, following the approach given in "von Mises yield function" section above. Figure 18 shows the corresponding information for a 15 % Bi-axial pre-strain [13].

It can clearly be seen that the instability strains change between having no pre-stain, (FLC), and either a 15 % tensile strain or a balanced bi-axial pre-strain. However, a single FLSC encompasses all the different strain conditions, (RHS graphs of Figs. 17 and 18). In principle, a matrix of tests can be conducted with varying levels of pre-strain in different strain path directions, and then the corresponding instability

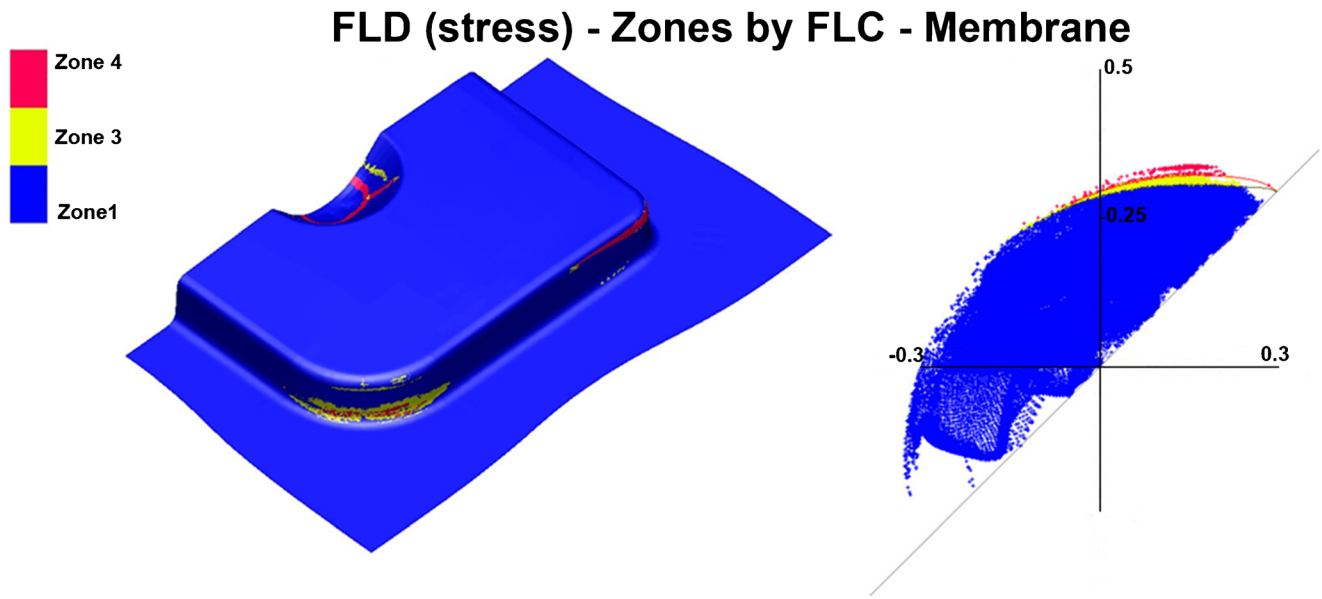

Fig. 13 FE simulation conducted using hill's 90 yield criterion with FLSD criterion

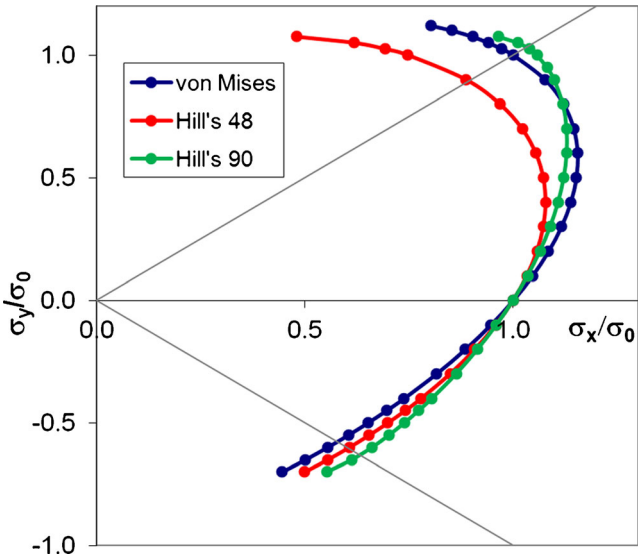

Fig. 14 Comparison of the different yield surfaces for an aluminium alloy. *Note*: Hill's 90 m value was 1.7

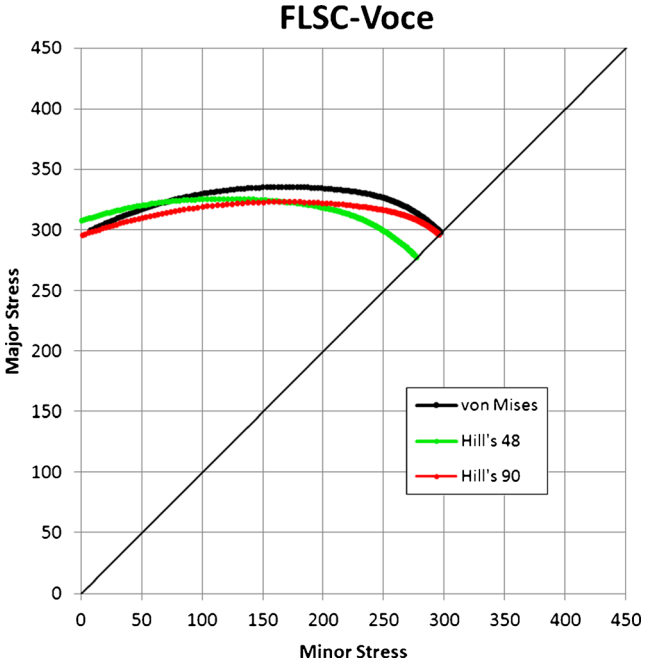

Fig. 16 Comparison of the different FLSD criteria using the different yield functions

strains determined over a range of strain paths. However, this would be a very time consuming and laborious task, as well as very expensive, for all materials and all gauges to be supplied. Also at this moment in time, although the strain path can be tracked within the FE software, multiple marginal and failure criteria can not be entered into the codes for a multitude of non-proportional strain paths. On the other hand, all non-proportional strain paths sensibly map to a single FLSC criterion which can be applied in current FE analysis, together with a safety margin offset, as demonstrated in this paper.

If a stamped sheet panel is pressed with sensibly proportional strain paths over the entire pressing, then it is quite acceptable and legitimate to use the conventional FLC approach, as has been carried out for many decades. However, any significant deviation from proportional strain paths will introduce significant errors, as shown in Figs. 17 and 18. Under these situations the FLSD approach, highlighted in this paper, may be successfully applied as demonstrated in sections "von Mises yield function", "Hill's 48 yield function", and "Hill's 90 yield function".

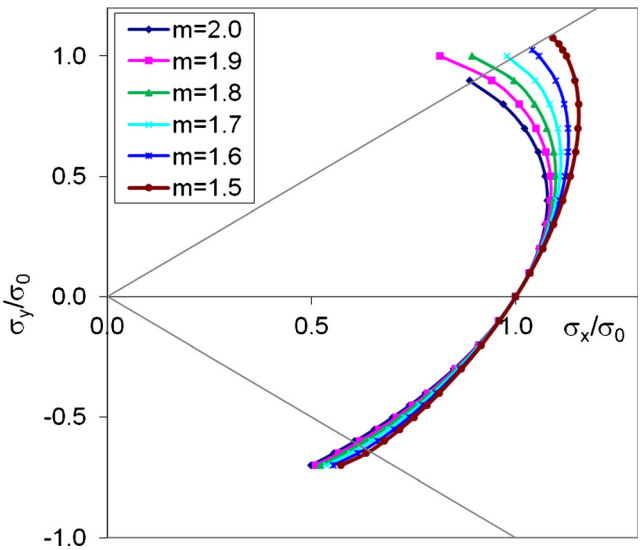

Fig. 15 Comparison of the different yield surfaces for an aluminium alloy produced by varying the m power in hill's 90 yield function

Summary

FLSD's presented in literature, based upon a steel FLC and a simple power law, usually have a "concave" type shape. The analysis presented in this paper, based upon a "flatter" aluminium FLC and a saturation stress Voce equation model, have shown "convex" shaped FLSD criteria.

The analysis in this paper, following on from the work Stoughton [16] and Bai &Wierzbicki [17], has demonstrated a method to transpose the strain based FLC into a stress based FLSD, using a Voce equation saturation stress constituent law together with the von Mises yield function.

This method was then successfully applied to two additional yield functions, namely Hill's 48, and Hill's 90. The same Voce equation saturation stress constituent law was used with each of the two additional yield functions.

FE stamping simulations were carried out, using the commercial code PamStamp, and good agreement was demonstrated between the traditional FLC analysis and the transposed FLSD analysis. Good agreement was generally demonstrated for all three yield functions considered in this paper,

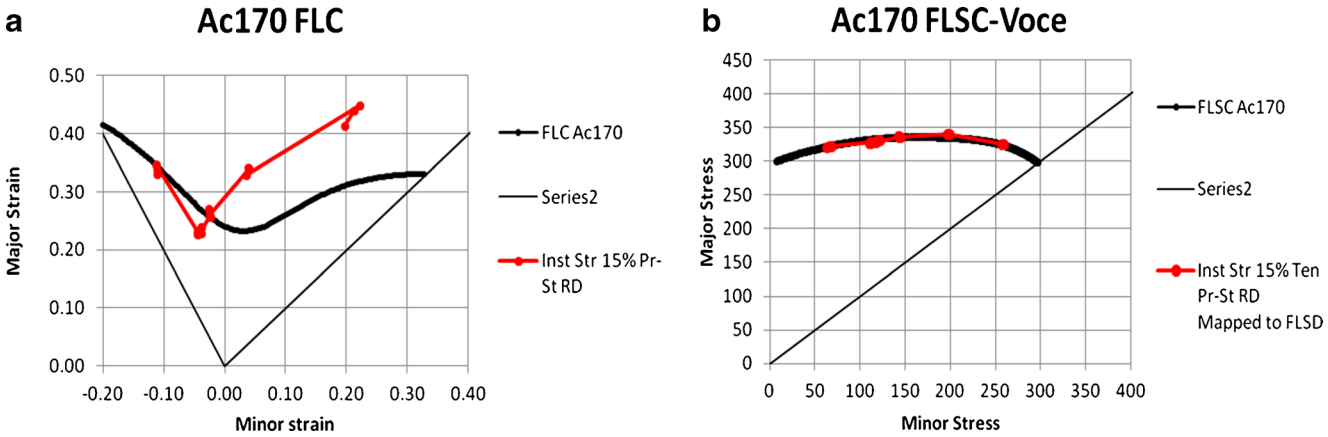

Fig. 17 Standard proportional strain path FLC (*Black*) & FLC determined after 15 % tensile pre-strain in the rolling direction (*Red*). Pre-strain data measurements carried out by Werber [25]

with some differences highlighted between Hill's 48 and Hill's 90 yield functions around the balanced bi-axial stress state.

Comparison of the results using the different yield functions has shown the reduced ability of Hill's 48 to predict correctly the balanced bi-axial failure zones for materials with an r value less than one, as compared to the von Mises and Hill's 90 yield functions. The lower predicted stress levels at the bi-axial state with Hill's 48, shown in Fig. 11, would predict a non failed FLSD region as compared to the failed FLC region in the central dome, (Figs. 7 and 8). It is known that Hill's 48 yield function does not give good agreement compared to experimental stress–strain data around the balanced bi-axial stress state, particularly for materials with an r value less than one, i.e. aluminium alloys. This relatively poor performance prompted Hill to derive his 90 criterion, which has been demonstrated to show both a failed FLC region and a failed FLSD region in the central dome, (Figs. 12 and 13).

The FLSD analysis has highlighted additional marginal/failure zones around the dies entry radius which are not present in the FLC analysis. Two of the yield functions considered in this paper predict marginal zones in this region, whilst that of Hill's 90 predicts a failed region. Therefore a cautious approach would need to be applied to the design of the component in this area on the basis of the presented analysis. However, the difference between the marginal and failed areas in the region of the die entry corner area, when applying the three yield functions considered, would need to be investigated experimentally to resolve the accuracy of the predictions from the FE analysis, and hence the accuracy of the three different yield functions in describing correctly the yield surface of the material considered.

The main drive to adopt an FLSD type criterion for FE analysis resides in the fact that the FLSD criterion is path independent. Hence, as demonstrated in this paper, only one FLC curve would need to be measured, for each material, and then transposed to an FLSD criterion for FE analysis. One remaining concern is that the FE calculation show lower accuracy in stress calculation than in strain calculation. Nevertheless this do not appears to be an issue in the present work as mentioned previously in "von Mises yield function" section.

Under the traditional FLC method, it would strictly be necessary to measure numerous "FLC's", starting with a series

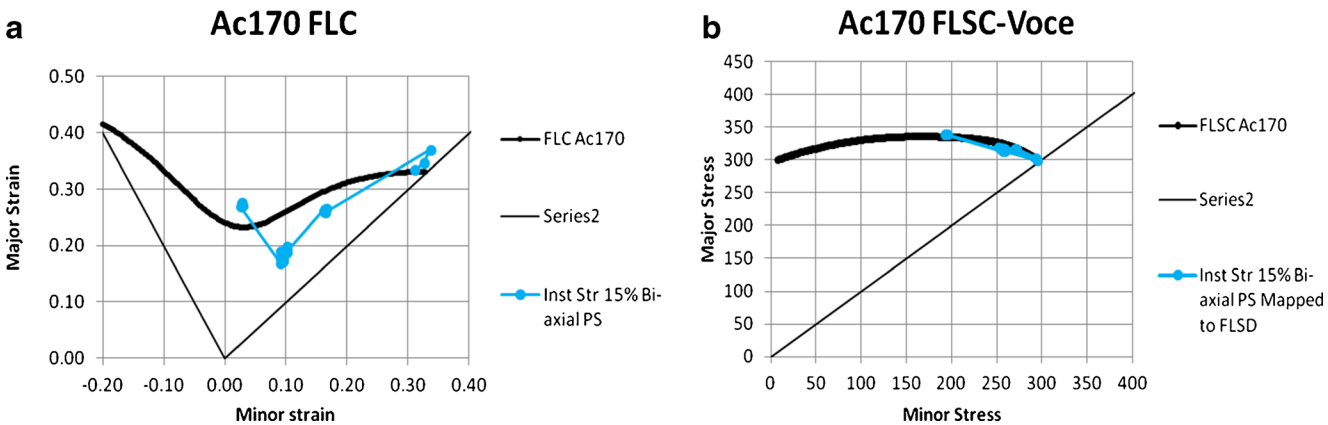

Fig. 18 Standard proportional strain path FLC (*Black*) & FLC determined after 15 % bi-axial pre-strain (*Blue*). Pre-strain measurements carried out by Werber [25]

of different pre-strains along differing initial strain paths, and then determining the final instability strains under the different strain ratios for each initial starting condition. This would be a very time consuming and a very expensive task. However, even if all this data was available, at present multiple marginal and failure criteria can not be entered into FE analysis codes for a multitude of non-proportional strain paths. However, it has been demonstrated that all non-proportional strain paths sensibly map to a single FLSC criterion which can be applied in current FE analysis codes together with a safety margin off-set.

In principle the type of analysis conducted in this paper with the currently use material models could be easily extended to higher order yield functions which have been developed over the last fifteen to twenty years, such as those presented in the literature for example by Barlat [23] and Banabic [24]. This is something which would be of great benefit as a number of the higher order yield functions, particularly the Barlat2000 and BBC05 functions, show a very good fit to the measured in-plane sheet properties, such as the r value and the stress value distributions.

The flow curve law used in the model as well should be adapted to more advanced models that best fit the data. Experimentally a saturation stress is not observed for the aluminium alloys studied here if we extend the flow curve using the biaxial data from the bulge test (see Fig. 11). Thus Voce law usually used should in the future be replaced in industry use by something more accurate like a Voce-Voce, a Gosh, or a Swift-Hockett-Sherby better fit.

As a final point, it should be remind that the transposed FLSD, derived from a unique measured FLC in the form of data pairs, have to be used only with the material models (yield function and flow curve) that were used to define the FLSD. Otherwise it will yield to inaccurate FE results.

Acknowledgments The authors would like to thank Mr. Corrado Bassi, Director, Automotive Development Europe, and Novelis Europe for permission to publish the above paper.

Also, the authors wish to thank Stuttgart University, and in particular Alexandra Werber, for permission to present some of their data [Private communication from J. Simon, Novelis, Sierre, Switzerland. Work carried out, and data generated, by Ph.D. student, Alexandra Werber, Stuttgart University.] in this paper.

References

1. Keeler SP, Backhofen WA (1964) Plastic instability and fracture in sheet stretched over rigid punches. ASM Trans Q 65:25–48
2. Goodwin GM (1968) Application of strain analysis to sheet metal forming in the press shop. SAE Pap. 680093
3. Graf A, Hosford W (1964) The influence of strain path changes on forming limit diagrams of AA6111-T4. Int J Mech Sci 36(10):897–910
4. Arrieux R, Bedrin C, Boivin M (1985) Determination of the strain path influence of the forming limit diagrams, from the limit stress curve. Ann CIRP Vol. 34/1/1985
5. Kohara S (1993) Forming-limit curves of aluminum and aluminum alloy sheets and effects of strain path on the curves. J Mat Process Tech 38:723–735
6. Yoshida K, Kuwabara T, Kuroda M (2007) Path-dependence of the forming limit stresses in a sheet metal. Int J Plast 23:361–384
7. Arrieux R, Bedrin C, Boivin M (1982) Determination of an intrinsic forming limit stress diagram for isotropic metal sheets. Proc of the 12th Bienn Congr of the IDDRG pp. 61–71
8. Arrieux R, Boivin M (1989) Theoretical determination of the forming limit stress curve for isotropic sheet materials. Ann CIRP Vol. 38/1/1989
9. Arrieux R (1995) Determination and use of the forming limit stress diagrams in sheet metal forming. J Mat Process Tech 53:4–56
10. Stoughton TB, Zhu X (2004) Review of theoretical models of the strain-based FLD and their relevance to the stress-based FLD. Int J Plast 20:1463–1486
11. Stoughton TB, Yoon JW (2005) Sheet metal formability analysis for anisotropic materials under non-proportional loading. Int J Mech Sci 47:1972–2002
12. Matin PH, Smith LM, Petrusevski S (2006) A method for stress space forming limit diagram construction for aluminum alloys. J Mat Process Tech 174:258–265
13. Chen MH, Gao L, Zuo DW, Wang M (2007) Application of the forming limit stress diagram to forming limit prediction for the multi-step forming of auto panels. J Mat Process Tech 187–188:173–177
14. Stoughton TB, Yoon JW (2011) A new approach for failure criterion for sheet metals. Int J Plast 27:440–459
15. Panich S, Uthaisangsuk V, Juntaratin J, Suranuntchai S (2011) Determination of forming limit stress diagram for formability prediction of SPCE 270 steel sheet. J Met Mat Miner 21(1):19–27
16. Stoughton TB (2000) A general forming limit criterion for sheet metal forming. IntJ Mech Sci 42(1):1–27
17. Bai Y, Wierzbicki T (2008) Forming severity concept for predicting sheet necking under complex loading histories. Int J Mech Sci 50:1012–1022
18. Johnson W, Mellor PB (1973) Engineering plasticity. Van Nostrand Reinhold Company Ltd., p87
19. Johnson W, Mellor PB (1973) Engineering plasticity. Van Nostrand Reinhold Company Ltd., p64
20. Hill R (1950) The mathematical theory of plasticity. Clarendon, Oxford
21. Johnson W, Mellor PB (1973) Engineering plasticity. Van Nostrand Reinhold Company Ltd. p96–97
22. Hill R (1990) Constitutive modelling of orthotropic plasticity in sheet metals. J Mech Phys Solids 38:405
23. Barlat F, Brem JC, Yoon JW, Chung K, Dick RE, Lege DJ, Pourboghrat F, Choi S-H, Chu E (2003) Plane stress yield function for aluminum alloy sheets—part 1: theory. Int J Plast 19:1297–1319
24. Banabic D, Balan T, Comsa DS (2000) A new yield criterion for orthotropic sheet metals under plane-stress condition. Proc. of the Conf. TPR2000 (Ed. Banabic D.), Cluj-Napoca, pp.217–224
25. Werber A, Simon J (2012) Private communication on Alexandra Werber's project at Stuttgart University